Sensitivity Derivatives of Flutter Characteristics and Stability Margins for Aeroservoelastic Design

M. Karpel*
Technion—Israel Institute of Technology, Haifa, Israel

Analytical derivatives of flutter dynamic pressure, flutter frequency, gain margins, and phase margins with respect to various aeroservoelastic design variables are developed. The formulation is based on a first-order time-domain aeroservoelastic mathematical model. The structure is represented in the model by vibration modes, the unsteady aerodymanics by minimum-state rational approximation functions, and the control system is coupled with the aeroelastic system through motion sensors and control surfaces. The sensitivity derivatives are expressed as exact functions of the stability boundary eigenvectors and of the real-valued system matrix derivatives with respect to arbitrary design variables. These expressions may be applied to any aeroservoelastic design variable with respect to which the system matrix derivative is available. System matrix derivatives with respect to structural stiffness and mass parameters, control gains, actuator parameters, and sensor locations are presented. The new sensitivity derivatives facilitate efficient gradient-based aeroservoelastic algorithms, which directly address flutter and stability margin requirements. A numerical example utilizing the mathematical model of the Active Flexible Wing wind-tunnel model is given. A practical control design problem with roll maneuver constraints is used to demonstrate the accuracy and usage of the derivatives.

Introduction

THE designer of a flight vehicle is required to show that the flutter speeds are sufficiently beyond the aircraft flight envelope and that the control system exhibits sufficient gain and phase margins. The aeroelastic mathematical models used to analyze the aeroelastic stability involve various disciplines such as structural properties, aerodynamics, payload distribution, and control system characteristics. The preliminary design of these disciplines usually starts with meeting basic performance and stress requirements. Stability characteristics are then analyzed and, if margin requirements are not satisfied, the design variables are to be changed to meet the required margins with a minimal performance penalty and without violating other constraints.

When the effect of the control system on flutter characteristics can be neglected and when the aerodynamic planform is not subjected to changes, the aeroelastic design variables are stiffness and mass distributions, and the penalty function is the total weight. The common approach for analyzing the aeroelastic system in this case is based on second-order frequency-domain formulation of the matrix equations of motion in modal coordinates.[1] Rudisill and Bhatia[2] used the second-order formulation to develop expressions for exact derivatives of the flutter speed with respect to structural design variables. Wilkinson et al.[3] extended these expressions and applied them to practical design of minimum-weight aircraft structures. These flutter derivatives were implemented in the FASTOP computer program[4] for combined flutter and strength optimization.

In many modern designs of high-maneuver flight vehicles, the interaction between the aeroelastic and the control systems cannot be neglected. The control system affects the flutter boundary, and the aeroelastic system affects the aircraft maneuver performance and the control gain and phase margins. Even though the aeroservoelastic system can still be analyzed using second-order formulation,[5] application of various modern control design techniques require the equations of motion to be cast in a first-order time-domain (state-space) form. Aeroservoelastic state-space models are based on rational approximation of the unsteady aerodynamic forces. Tiffany and Adams[6] reviewed and extended various approximation methods and applied them in NASA's Interaction of Structures, Aerodynamics, and Controls (ISAC) computer program. Among those, the minimum-state method of Karpel[7,8] yields a required level of accuracy with a minimal number of states.

State-space aeroservoelastic models have been used in various applications of optimal (full-state feedback) and reduced-order control techniques such as those of Abel et al.[9] and Mukhopadhyay et al.[10] These techniques are based on the minimization of the sum of weighted mean-square response parameters. Zeiler and Weisshaar[11] performed simultaneous structural and control optimization by utilizing the multilevel decomposition technique of Sobieszczanski-Sobieski et al.[12] and minimizing a stability index based on the system eigenvalues. Even though these methods result in stable systems, they do not address flutter speed and control gain and phase margins directly. As a result, the solutions may exhibit low safety margins, which indicate low robustness.

The main purpose of this work is to develop analytical expressions for exact derivatives of the flutter dynamic pressure, flutter frequency, and gain and phase margins with respect to structural and control design variables, based on state-space formulation. This facilitates an efficient inclusion of the flutter and stability margins as part of the objective function and the constraint equations in any gradient-based design algorithm dealing with aeroservoelastic systems.

Equations of Motion

The equations of motion in this paper follow the time-domain aeroservoelastic modeling technique of Ref. 8. The Laplace transform of the open-loop aeroelastic system equation of motion, excited by control surface motion reads

$$([M_s]s^2+[B_s]s+[K_s]+q[Q_s(s)])\{\xi(s)\}$$
$$+([M_c]s^2+q[Q_c(s)])\{\delta(s)\}=\{0\} \quad (1)$$

where $[M_s]$, $[B_s]$, and $[K_s]$ are the generalized structural mass, damping, and stiffness matrices respectively, $[M_c]$ is the coupling mass matrix between the control and the structural

Received March 20, 1989; revision received Sept. 12, 1989.

*Senior Research Fellow, Faculty of Aerospace Engineering; presently, NRC Research Associate, NASA Langley Research Center, Hampton, VA.

modes, $\{\xi\}$ is the vector of generalized structural displacements, $\{\delta\}$ is the vector of control surface commanded deflections, namely the actuator outputs (in radians), $[Q_s]$ and $[Q_c]$ are the unsteady aerodynamic force matrices associated with the structural and the control modes, and q is the dynamic pressure. In order to transform Eq. (1) into a time-domain constant coefficient equation, the aerodynamic matrices have to be described as rational functions of s. The minimum-state method[7,8] approximates $[Q(s)]$ by

$$[\bar{Q}(\bar{s})] = [A_0] + [A_1]\bar{s} + [A_2]\bar{s}^2 + [D](\bar{s}[I] - [R])^{-1}[E]\bar{s} \quad (2)$$

where $\bar{s}$ is the nondimensionalized Laplace variable $\bar{s} = sb/V$, b is the reference semichord, V is the true air speed, $[R]$ is a diagonal matrix with distinct negative terms representing the aerodynamic lags, and $[D]$ and $[E]$ are aerodynamic coupling matrices between the modal and aerodynamic states (as shown below). The real-valued approximation matrices of Eq. (2) are partitioned into structural and control mode related terms as

$$[A_i] = [A_{s_i}\ A_{c_i}] \qquad \text{for } i = 0,1,2 \quad (3a)$$

$$[D] = [D_s] \quad (3b)$$

$$[E] = [E_s\ E_c] \quad (3c)$$

The resulting time-domain, state-space, open-loop aeroelastic plant equation of motion is

$$\{\dot{x}_p\} = [A_p]\{x_p\} + [B_p]\{u_p\} \quad (4)$$

where

$$\{x_p\} = \begin{Bmatrix} \xi \\ \dot{\xi} \\ x_a \end{Bmatrix}; \qquad \{u_p\} = \begin{Bmatrix} \delta \\ \dot{\delta} \\ \ddot{\delta} \end{Bmatrix} \quad (5a)$$

$$[A_p] = \begin{bmatrix} 0 & I & 0 \\ -\bar{M}_s^{-1}(K_s + qA_{s_0}) & -\bar{M}_s^{-1}\left(B_s + \dfrac{qb}{V}A_{s_1}\right) & -q\bar{M}_s^{-1}D \\ 0 & E_s & \dfrac{V}{b}R \end{bmatrix} \quad (5b)$$

$$[B_p] = \begin{bmatrix} 0 & 0 & 0 \\ -q\bar{M}_s^{-1}A_{c_0} & -\dfrac{qb}{V}\bar{M}_s^{-1}A_{c_1} & -\bar{M}_s^{-1}\left(M_c + \dfrac{qb^2}{V^2}A_{c_2}\right) \\ 0 & E_c & 0 \end{bmatrix} \quad (5c)$$

where

$$[\bar{M}_s] = [M_s] + \frac{qb^2}{V^2}[A_{s_2}]$$

and $\{x_a\}$ is the vector of aerodynamic states.

The actuator transfer functions can also be expressed in a state-space form[10] as

$$\{\dot{x}_{ac}\} = [A_{ac}]\{x_{ac}\} + [B_{ac}]\{u\} \quad (6a)$$

$$\{u_p\} = [C_{ac}]\{x_{ac}\} \quad (6b)$$

where $[A_{ac}]$, $[B_{ac}]$, and $[C_{ac}]$ are the dynamic matrix, the control distribution matrix, and the output matrix of the actuators, and $\{u\}$ is the actuator command inputs. The order of the actuator state vector is the sum of the orders of the denominators in the actuator transfer functions. It is assumed here that the actuators are irreversible, which means that the control surface hinge moments have negligible effect on the actuator dynamics. The plant state vector of Eq. (4) can be augmented by the actuator states, which yields

$$\{\dot{x}\} = [A]\{x\} + [B]\{u\} \quad (7a)$$

$$\{y\} = [C]\{x\} \quad (7b)$$

where

$$\{x\} = \begin{Bmatrix} x_p \\ x_{ac} \end{Bmatrix}; \qquad [A] = \begin{bmatrix} A_p & B_pC_{ac} \\ 0 & A_{ac} \end{bmatrix}; \qquad [B] = \begin{bmatrix} 0 \\ B_{ac} \end{bmatrix}$$

and where $\{y\}$ is the sensor reading vector. It is assumed here, for the sake of simplicity, that the sensor dynamics may be neglected. The sensors, which are relevant to aeroservoelastic analysis, are usually either angular velocity meters or accelerometers. The $[C]$ matrices associated with these sensors are

$$[C_v] = [0 \quad \Phi'^T \quad 0 \quad 0] \quad (8a)$$

and

$$[C_a] = [0 \quad \Phi^T \quad 0 \quad 0]\,[A] \quad (8b)$$

where $[\Phi]$ and $[\Phi']$ the modal deflection and slope matrices at the sensor inputs and the column partitions are associated with the state components $\{\xi\}$, $\{\dot{\xi}\}$, $\{x_a\}$, and $\{x_{ac}\}$.

Equation (7) is the starting point for designing a control system for the given plant, which adds control states that can be augmented to the state vector. For the purposes of this paper, the actuator portion of Eqs. (7), being independent of flight conditions, is regarded as representing other control system components such as the electronic components and the sensors. The open loop or Eqs. (7) can be closed via a gain matrix $[G]$ that relates $\{u\}$ to $\{y\}$, which results in the closed-loop equation

$$\{\dot{x}\} = [\bar{A}]\{x\} \quad (9)$$

where

$$[\bar{A}] = [A] + [B]\,[G]\,[C]$$

Flutter Characteristics and Stability Margins

The flutter characteristics of Eq. (9) are found by calculating the complex eigenvalues of $[\bar{A}]$ at various values of dynamic pressure (q) with fixed Mach number (which defines the aerodynamic force matrices) and true air speed. The flutter dynamic pressure (q_f) is the lowest q at which the real part of any eigenvalue $\mathrm{Re}(\lambda_f)$ crosses the zero line to the right side of the Laplace domain. The flutter frequency ω_f is the value of the imaginary part of the flutter eigenvalue $\mathrm{Im}(\lambda_f)$. The flutter margin associated with the design dynamic pressure q_d is defined as

$$FM = (q_f - q_d)/q_d \quad (10)$$

A typical dynamic pressure margin requirement is 0.44 (equivalent to velocity margin of 0.2 required by aviation regulations).

Additional safety margins are required when the control system is involved. A positive gain margin for a nonzero term (G_{ij}) of the gain matrix may be conveniently found by setting $q = q_d$ and calculating the root-loci where the magnitude of G_{ij} is increased starting from its nominal value (G_{ij_n}) until instability occurs at $G_{ij} = G_{ij}^*$. The gain margin is defined as

$$GM_{ij} = 20 \log (G_{ij}^*/G_{ij_n}) \quad (11)$$

The negative gain margin is found by decreasing the magnitude of G_{ij} until instability occurs. It is assumed here that the system is stable at q_d and the G_{ij_n} and G_{ij}^* have the same sign.

A phase margin for each nonzero gain is found by setting $q = q_d$ and $G_{ij} = G_{ij_n} e^{i\theta_{ij}}$ and by calculating the root loci with increasing magnitudes of the phase shift θ_{ij} (positive and negative) until instability occurs at $\theta_{ij} = \theta_{ij}^*$. The gain margin is defined as

$$PM_{ij} = -(360/2\pi)\,\theta_{ij}^* \tag{12}$$

Typical aviation regulation gain and phase margin requirements are $|GM| \geq 6$ dB and $|PM| \geq 60$ deg.

In an automated, gradient-based design process, where stability parameters are calculated at each design step, the flutter and stability margin derivatives defined in the following sections may be used to estimate the next-point stability boundary parameters.

Flutter Derivatives

Once q_f and ω_f are known, an eigenvector extraction routine can be used to calculate the associated complex column eigenvector $\{X_f\}$ and row eigenvector $\{\bar{X}_f\}$ which satisfy

$$([\bar{A}(q_f)] - \lambda_f[I])\{X_f\} = \{0\} \tag{13}$$

and

$$\{\bar{X}_f\}^T([\bar{A}(q_f)] - \lambda_f[I]) = \{0\}^T \tag{14}$$

where $\lambda_f = i\omega_f$ is the flutter eigenvalue and $[I]$ is a unit matrix. The differentiation of Eq. (13) with respect to a design parameter p_k, premultiplication by $\{\bar{X}_f\}^T$, and the use of Eq. (14) to nullify the $\partial\{X\}/\partial p_k$ term yield

$$\frac{\partial\lambda}{\partial p_k} = \frac{\{\bar{X}_f\}^T \dfrac{\partial[\bar{A}(q_f)]}{\partial p_k}\{X_f\}}{\{\bar{X}_f\}^T\{X_f\}} \tag{15}$$

In the same way, the eigenvalue derivative with respect to the dynamic pressure is

$$\frac{\partial\lambda}{\partial q} = \frac{\{\bar{X}_f\}^T \left.\dfrac{\partial[\bar{A}(q)]}{\partial q}\right|_{q=q_f}\{X_f\}}{\{\bar{X}_f\}^T\{X_f\}} \tag{16}$$

The system matrix derivatives on the right side of Eqs. (15) and (16) are discussed in the next section. The differential increment of λ due to simultaneous incremental changes in q and in p_k is

$$d\lambda = \frac{\partial\lambda}{\partial q}\,dq + \frac{\partial\lambda}{\partial p_k}\,dp_k \tag{17}$$

Equation (17) is a complex equation. When $d\lambda$ is pure imaginary ($d\lambda = i\,d\omega_f$), dq is the incremental change in q_f. The real part of Eq. (17) in this case yields the flutter dynamic pressure derivatives

$$\frac{\partial q_f}{\partial p_k} = -\frac{\mathrm{Re}(\partial\lambda/\partial p_k)}{\mathrm{Re}(\partial\lambda/\partial q)} \tag{18}$$

and the imaginary part of Eq. (17) yields the flutter frequency derivatives

$$\frac{\partial\omega_f}{\partial p_k} = \mathrm{Im}\left(\frac{\partial\lambda}{\partial q}\right)\frac{\partial q_f}{\partial p_k} + \mathrm{Im}\left(\frac{\partial\lambda}{\partial p_k}\right) \tag{19}$$

It should be noted that the only design parameter dependent term in the flutter derivative expressions of Eqs. (18) and (19) is $\partial\lambda/\partial p_k$, which can be calculated by Eq. (15) using the same eigenvectors for any design parameter with respect to which the system matrix derivative is available.

System Matrix Derivatives

Dynamic Pressure

The close-loop system matrix $[\bar{A}]$ can be partitioned as

$$[\bar{A}] = \begin{bmatrix} A^{(1)} \\ A^{(2)} \\ A^{(3)} \\ A^{(4)} + B_{ac}GC \end{bmatrix} \tag{20}$$

where the $[A^{(i)}]$ matrices are the $\dot{\xi}$, $\ddot{\xi}$, $\dot{x}_a$, and $\dot{x}_{ac}$ related partitions of $[A]$ of Eq. (7). The $[A^{(1)}]$, $[A^{(3)}]$, and $[A^{(4)}]$ are not a function of q. The $[A^{(2)}]$ can be expressed as

$$[A^{(2)}] = -[\bar{M}_s]^{-1}[\tilde{A}^{(2)}] \tag{21}$$

where $[\bar{M}_s]$ is defined in Eq. (5) and where

$$[\tilde{A}^{(2)}] = \left[K_s + qA_{s_0} \quad B_s + \frac{qb}{V}A_{s_1} \quad qD \quad q\tilde{A}_{c_0} \quad \frac{qb}{V}\tilde{A}_{c_1} \quad \tilde{M}_c + \frac{qb^2}{V^2}\tilde{A}_{c_2}\right]$$

where the $\sim$ terms in the right side are those of $[B_p]$ of Eq. (5c) postmultiplied by $[C_{ac}]$ as done in Eq. (7). The differentiation of Eq. (21) with respect to q yields

$$\frac{\partial[A^{(2)}]}{\partial q} = -[\bar{M}_s]^{-1}\left(\frac{b^2}{V^2}[A_{s_2}]\,[A^{(2)}] + \frac{\partial[\tilde{A}^{(2)}]}{\partial q}\right) \tag{22}$$

where

$$\frac{\partial[\tilde{A}^{(2)}]}{\partial q} = \left[A_{s_0} \quad \frac{b}{V}A_{s_1} \quad D \quad \tilde{A}_{c_0} \quad \frac{b}{V}\tilde{A}_{c_1} \quad \frac{b^2}{V^2}\tilde{A}_{c_2}\right]$$

The derivative of $[\bar{A}]$ with respect to q, based on Eqs. (8), (20), and (22) is

$$\frac{\partial[\bar{A}]}{\partial q} = \begin{bmatrix} 0 \\ \partial A^{(2)}/\partial q \\ 0 \\ B_{ac}G\Phi\partial A^{(2)}/\partial q \end{bmatrix} \tag{23}$$

where the bottom partition is nonzero only when there are active acceleration measurements.

Structural Parameters

The structure is represented in the basic aeroservoelastic model by a limited set of low-frequency natural vibration modes calculated from a full-size finite-element model. The mode shapes serve as generalized coordinates, and the generalized masses, stiffnesses, and dampings construct the diagonal $[M_s]$, $[K_s]$, and $[B_s]$ matrices of Eq. (5), respectively. These properties change when the structural model is modified. However, if enough modes are taken into account and if the structural changes are not too large, it may be assumed that the structural deflections after modifications are still a linear combination of the original generalized coordinates. Structural changes are introduced to the aeroservoelastic model in this case by modifying $[M_s]$ and $[K_s]$ (which become nondiagonal) without changing the modal coordinates. This assumption is used in many applications such as the optimization methods of Refs. 2-4 and 14. The validity of the assumption can be checked by comparing the flutter characteristics at the end of the resizing process with those obtained by performing flutter analysis with the new modes calculated from the modified, finite-element model.

Differentiation of Eq. (21) with respect to an arbitrary design variable p_{s_i} that affects the stiffness and/or mass properties yields

$$\frac{\partial[A^{(2)}]}{\partial p_{s_i}} = -[\bar{M}_s]^{-1}\left(\frac{\partial[M_s]}{\partial p_{s_i}}[A^{(2)}] + \begin{bmatrix}\frac{\partial[K_s]}{\partial p_{s_i}} & 0 & 0 & 0 & \frac{\partial[\tilde{M}_c]}{\partial p_{s_i}}\end{bmatrix}\right) \tag{24}$$

where the derivatives on the right side are

$$\frac{\partial[K_s]}{\partial p_{s_i}} = [\Psi_m]^T \frac{\partial[K]}{\partial p_{s_i}}[\Psi_m] \tag{25a}$$

$$\frac{\partial[M_s]}{\partial p_{s_i}} = [\Psi_m]^T \frac{\partial[M]}{\partial p_{s_i}}[\Psi_m] \tag{25b}$$

$$\frac{\partial[\tilde{M}_c]}{\partial p_{s_i}} = [\Psi_m]^T \frac{\partial[M]}{\partial p_{s_i}}[\tilde{\Psi}_c] \tag{25c}$$

where $[K]$ and $[M]$ are the discrete-coordinate, finite-element stiffness and mass matrices, $[\Psi_m]$ is the vibration mode matrix, and $[\tilde{\Psi}_c]$ is the control surface deflections matrix postmultiplied by the appropriate terms of $[C_{ac}]$ of Eqs. (7). For most commonly used structural design variables, such as thin element gages and lumped masses, the stiffness and mass matrices are linear with p_{s_i} and their derivatives are simply

$$\frac{\partial[K]}{\partial p_{s_i}} = \frac{[K_i]}{p_{s_i}} \tag{26a}$$

$$\frac{\partial[M]}{\partial p_{s_i}} = \frac{[M_i]}{p_{s_i}} \tag{26b}$$

where $[K_i]$ and $[M_i]$ are zero matrices except for the terms associated with p_{s_i}. In this case, $[K_i]/p_{s_i}$ and $[M_i]/p_{s_i}$ and the resulting derivatives of Eqs. (25) are not a function of p_{s_i} itself. When p_{s_i} is involved with significant geometrical changes, $[K]$ and $[M]$ may not be linear functions of p_{s_i}, and different expressions for their derivatives, which are beyond the scope of this paper, should be used in lieu of Eqs. (26).

Here again, $[A^{(1)}]$, $[A^{(3)}]$, and $[A^{(4)}]$ are not a function of p_{s_i} and

$$\frac{\partial[\bar{A}]}{\partial p_{s_i}} = \begin{bmatrix} 0 \\ \partial A^{(2)}/\partial p_{s_i} \\ 0 \\ B_{ac} G \Phi \partial A^{(2)}/\partial p_{s_i} \end{bmatrix} \tag{27}$$

where the bottom partition is nonzero only when there are active acceleration measurements.

Control System Parameters

The control system design parameters appear only at the bottom partition of $[\bar{A}]$ in Eq. (20) and they may be categorized according to the matrix components that they affect. The categories are 1) control gains which affect the gain matrix $[G]$, 2) control system dynamics parameters which are represented in this paper by the actuator matrices $[A_{ac}]$ and $[B_{ac}]$, and 3) sensor locations which affect the output matrix $[C]$.

The derivative of $[\bar{A}]$ with respect to a control gain G_{ij}, which connects the ith actuator with the jth sensor is

$$\frac{\partial[\bar{A}]}{\partial G_{ij}} = \begin{bmatrix} 0 \\ 0 \\ 0 \\ B_{ac_i} C_j \end{bmatrix} \tag{28}$$

where B_{ac_i} is the ith column of $[B_{ac}]$ and C_j is the jth row of $[C]$.

The derivative of $[\bar{A}]$ with respect to a control system dynamics parameter p_{ac_i} is

$$\frac{\partial[\bar{A}]}{\partial p_{ac_i}} = \begin{bmatrix} 0 \\ 0 \\ 0 \\ \begin{bmatrix} 0 & \frac{\partial A_{ac}}{\partial p_{ac_i}} \end{bmatrix} + \frac{\partial B_{ac}}{\partial p_{ac_i}} GC \end{bmatrix} \tag{29}$$

The structure of $[A_{ac}]$ and $[B_{ac}]$ depend on the specific nature of the control component and the associated state-space modeling technique. Various examples may be found in linear system books such as that of Kailath.[15] The design variables usually appear in the control system matrices in an explicit and easy to differentiate form.

The derivative of $[\bar{A}]$ with respect to the ith location coordinate of the jth sensor $p_{m_{ij}}$ is

$$\frac{\partial[\bar{A}]}{\partial p_{m_{ij}}} = \begin{bmatrix} 0 \\ 0 \\ 0 \\ B_{ac} G_j \frac{\partial C_j}{\partial p_{m_{ij}}} \end{bmatrix} \tag{30}$$

where G_j is the jth column of $[G]$, and $\partial C_j/\partial p_{m_{ij}}$ is obtained by differentiating the jth row of $[\Phi]$ or $[\Phi']$ of Eqs. (8) with respect to the relevant location coordinate, which can be performed by standard spline interpolation routines.

Stability Margin Derivatives

The process of calculating the derivatives of a gain margin associated with G_{ij} starts with finding the value of $G_{ij} = G_{ij}^*$, which causes flutter at $q_f^* = q_d$, and calculating the gain margin GM_{ij} using Eq. (11). Since G_{ij}^* is not a function of G_{ij} itself, the differentiation of Eq. (11) with respect to G_{ij} yields

$$\frac{\partial GM_{ij}}{\partial G_{ij}} = -\frac{20/\ell n\ 10}{G_{ij_n}} \tag{31}$$

The differentiation of Eq. (11) with respect to another design variable (which may be another gain) yields

$$\frac{\partial GM_{ij}}{\partial p_k} = -\frac{20/\ell n\ 10}{G_{ij}^*}\frac{\partial G_{ij}^*}{\partial p_k} \tag{32}$$

The incremental change of q_f^* due to simultaneous changes of G_{ij} (from $G_{ij} = G_{ij}^*$) and p_k (from its nominal value) is

$$\mathrm{d}q_f^* = \frac{\partial q_f^*}{\partial G_{ij}}\mathrm{d}G_{ij} + \frac{\partial q_f^*}{\partial p_k}\mathrm{d}p_k \tag{33}$$

When $\mathrm{d}q_f^* = 0$, $\mathrm{d}G_{ij}$ is actually $\mathrm{d}G_{ij}^*$, which yields

$$\frac{\partial G_{ij}^*}{\partial p_k} = -\frac{\partial q_f^*/\partial p_k}{\partial q_f^*/\partial G_{ij}} \tag{34}$$

Substitution in Eq. (32) gives

$$\frac{\partial GM_{ij}}{\partial p_k} = -\frac{20/\ell n\ 10}{G_{ij}^*}\frac{\partial q_f^*/\partial p_k}{\partial q_f^*/\partial G_{ij}} \tag{35}$$

where the derivatives on the right side are calculated like those of the flutter dynamic pressure in Eqs. (13) to (18) but with q_d and G_{ij}^* replacing q_f and G_{ij} in the system matrix, which requires a new set of flutter eigenvectors.

The process of calculating the derivatives of a phase margin associated with G_{ij} starts with finding the phase shift $\theta_{ij} = \theta_{ij}^*$, which causes flutter at $q_f^* = q_d$. The differentiation of Eq. (12) with respect to p_k yields

$$\frac{\partial PM_{ij}}{\partial p_k} = -\frac{360}{2\pi}\frac{\partial \theta_{ij}^*}{\partial p_k} \tag{36}$$

Similarly to the development of Eq. (34)

$$\frac{\partial \theta_{ij}^*}{\partial p_k} = -\frac{\partial q_f^*/\partial p_k}{\partial q_f^*/\partial \theta_{ij}} \tag{37}$$

The $\partial q_f^*/\partial \theta_{ij}$ can be calculated by Eq. (18) with $\partial\lambda/\partial p_k$ replaced by

$$\frac{\partial \lambda^*}{\partial \theta_{ij}} = iG_{ij_n}e^{i\theta_{ij}^*}\frac{\partial \lambda^*}{\partial G_{ij}} \tag{38}$$

Equations (18) and (36–38) yield

$$\frac{\partial PM_{ij}}{\partial p_k} = -\frac{360}{2\pi}\frac{\partial q_f^*/\partial p_k}{G_{ij_n}} \times \frac{\mathrm{Re}(\partial\lambda^*/\partial q)}{\mathrm{Im}(\partial\lambda^*/\partial G_{ij})\cos(\theta_{ij}^*) + \mathrm{Re}(\partial\lambda^*/\partial G_{ij})\sin(\theta_{ij}^*)} \tag{39}$$

where the derivatives on the right side are calculated using Eqs. (13–18) with $q = q_d$ and G_{ij} shifted by θ_{ij}^*.

Application to Control Gain Design

Mathematical Model and Definition of the Problem

The numerical application deals with Rockwell's Active Flexible Wing (AFW) wind-tunnel model to be tested at the Transonic Dynamics Tunnel, NASA Langley Research Center. A top view of the aerodynamic model is given in Fig. 1. The circles indicate points at which modal data were obtained from the vibration analysis. The mathematical model consists of 10 antisymmetric modes: 1 rigid-body (roll), 5 elastic, and 4 control-surface deflection modes. The minimum-state method of Ref. 8 is used to approximate the Mach 0.9 doublet lattice tabulated, generalized, unsteady aerodynamic matrices with four approximation roots, which yields four aerodynamic augmented states. Four third-order irreversible actuators are used to drive the control surfaces. The constant gain (zero-order) control system reads a single roll-rate measurement and commands each actuator according to its assigned control gain. The total order of the closed-loop system is 28 (12 structural, 4 aerodynamic, and 12 actuator states). An open-loop flutter analysis results in $q_f = 1.943$ psi and $\omega_f = 87.1$ rad/s.

The design dynamic pressure is $q_d = 1.5$ psi. The rigid and the aeroelastically flexibilized aerodynamic rolling moment coefficients (rigid L_{δ_i}/q and elastic L_{δ_i} at q_d) associated with the control surfaces of Fig. 1 are given in Table 1, where the control effectiveness values are calculated using the modal method of Ref. 13 with 11 vibration modes. A performance analysis established that a control law which supplies a rolling moment of -3000 lb-in. per unit aircraft roll velocity (minus pilot roll command) is required for adequate roll performance at q_d. Since the inboard trailing-edge control surface (2) is much more effective than the others, a control law which activates this control surface only has been designed first. However, this "start-point" control law yields closed-loop flutter at $q_f = 1.382$ psi, which is of course unacceptable. The start-point root-loci are shown in Fig. 2.

The design objective in this paper is to find the set of zero-order control gains that yield the best combination of closed-loop flutter and stability margins where the control gains are limited to a maximum absolute value of less than 0.16 rad/(rad/s) and where they are constrained to yield the required rolling moment of

$$\sum_i G_i L_{\delta_i} = -3000 \tag{40}$$

Another practical design guideline is to avoid the activation of control surfaces whose contributions to the design objectives are insignificant. Since there is only one sensor, the second subscript of G_{ij} of the preceding sections is omitted in this section. The constraint of Eq. (40) calls for the definition of a dependent variable. Since G_2 is the most effective in roll, it is chosen to be the dependent variable, such that control surface 2 compensates for the change in total rolling moment due to the activation of other control surfaces. The constrained differentiation operators with respect to the remaining independent design variables become

$$\frac{\partial}{\partial \tilde{G}_i} = \frac{\partial}{\partial G_i} - \frac{L_{\delta_i}}{L_{\delta_2}}\frac{\partial}{\partial G_2} \tag{41}$$

Three cases with different design strategies, which provide physical insight and demonstrate the accuracy and usage of the sensitivity derivatives, are described in the following subsections.

Table 1 Aerodynamic control-surface rolling moment coefficients and static aeroelastic effects

Control surface no.	Rigid L_{δ_i}/q (in.^{3}/rad)	Effectiveness at $q = 1.5$ psi	Elastic L_{δ_i} (lb-in./rad)
1	189	20.05	5,681
2	25,233	0.64	24,261
3	670	5.87	5,901
4	22,274	0.27	8,921

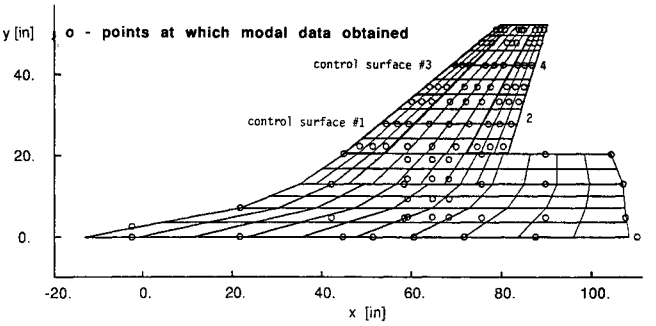

Fig. 1 Top view of the AFW aerodynamic model and structural grids.

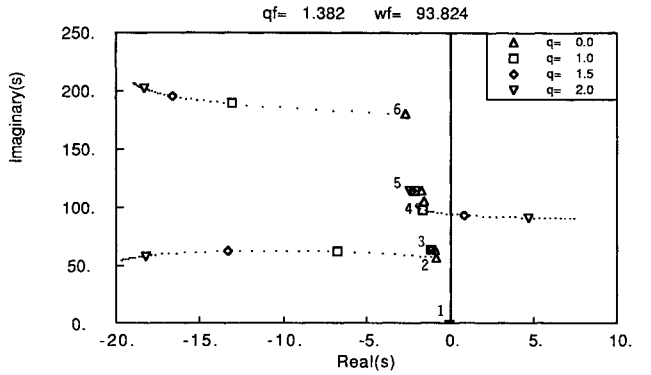

Fig. 2 Design start-point closed-loop root loci.

Design for Flutter Margins Only

The objective in this case is to increase the closed-loop flutter-dynamic pressure as much as possible subject to the

preceding design limits and constraints. The start-point control gains and the derivatives of q_f with respect to the constrained and the unconstrained gains are given in Table 2. It can be observed that the outboard trailing-edge control surface (4) has a much larger effect on flutter than the others at this point. Consequently, the design strategy in this case is to advance in steps where $G_1 = G_3 = 0$ and G_4 is changed to produce an expected q_f increase of 0.1 psi in each step. The value of the dependent design variable along the design path is $G_2 = -0.124 - 0.368G_4$ where -0.124 is the start-point value, and 0.368 is the ratio between L_{δ_4} and L_{δ_2} of Table 1.

The variations of q_f and ω_f along the design path are shown in Figs. 3 and 4, respectively. The actual calculated values at each point are compared in these figures to those expected based on previous-point calculated values and their derivatives. It can be observed that the region of $G_4 = 0.065$ to 0.075 is a transition region in which there is a change in the flutter mechanism. At $G_4 = 0.067$, the procedure does not anticipate this change and makes a relatively large step to $G_4 = 0.086$. The same modes (2 and 4 of Fig. 2) are still involved in the flutter mechanism, but branch 2 is now the one that crosses the imaginary axis with a large drop in q_f and ω_f. From this point the design is driven back to the point of maximum q_f ($G_4 = 0.07$, $G_2 = -0.15$, $q_f = 2$ psi) and terminates. The dashed lines plotted in Figs. 3 and 4 between actual flutter parameters and those expected at the next design point demonstrate the accuracy of the analytical derivatives of the flutter characteristics. Significant errors in this first-order prediction of next-step q_f and ω_f occur only in the transition region where the derivatives change rapidly. The derivatives of q_f with respect to the independent design variables are given in Fig. 5. It can be observed that $\partial \tilde{q}_f / \partial G_4$ is the largest one along the entire design path. The gain and phase margins vs G_4 are given in Figs. 6 and 7. Even though the end design point of this case ($G_4 = 0.07$) yields the maximal q_f, it shows poor gain and phase margins.

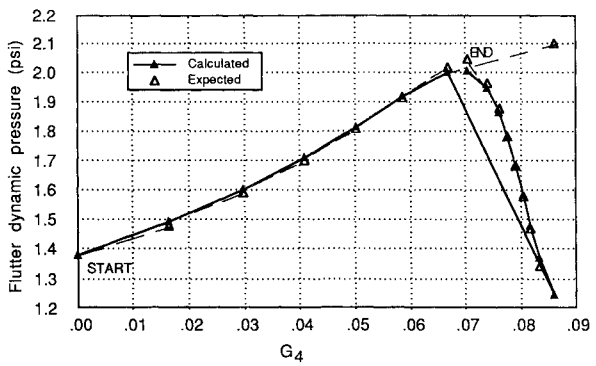

Fig. 3 Calculated and expected variations of flutter dynamic pressure along the design path.

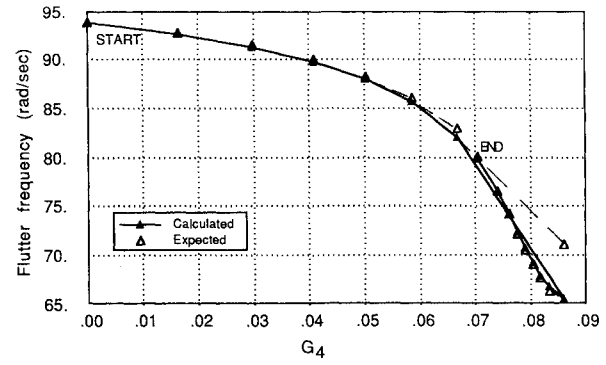

Fig. 4 Calculated and expected variations of flutter frequency along the design path.

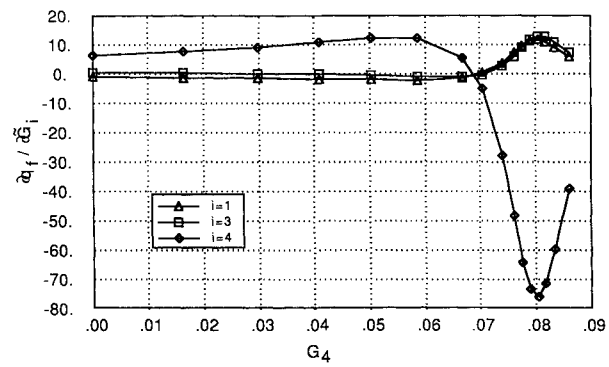

Fig. 5 Constrained derivatives of the flutter dynamic pressure along the design path.

Design for Flutter and Gain Margins

The design objective now is to find the set of gains that yields the least violation of the typical margin requirements given before ($FM \geq 0.44$, $|GM| \geq 6$ dB, $|PM| \geq 60$ deg). The inspection of Figs. 3, 6, and 7 indicates that such set (with $G_1 = G_3 = 0$) would be $G_2 = -0.145$ and $G_4 = -0.057$, which yields $FM = 0.27$, $GM_2 = GM_4 = 2.9$ dB, and $PM_4 = 47$ deg.

In order to demonstrate the stability margin derivatives and their use in a design process, we now attempt to find the optimal gain set in an automated process that does not "know" the findings of the previous design case. since the phase margin and the negative gain margin violation of the typical requirements has been shown to be consistently lower than those of the positive gain margins (see Figs. 6 and 7), only flutter and positive gain margins appear in the objective function:

$$J = \frac{0.1}{FM} + \frac{1}{GM_m} \tag{42}$$

where

$$GM_m = \min_i \{GM_i\}$$

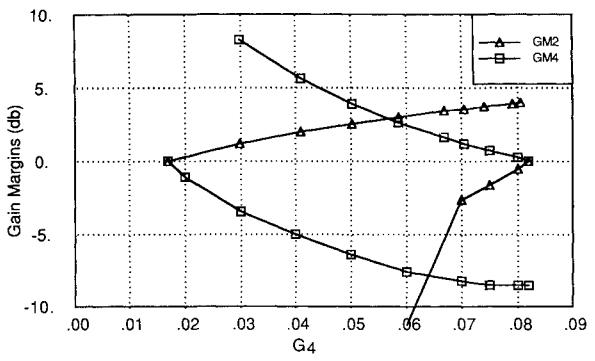

Fig. 6 Gain margins along the design path.

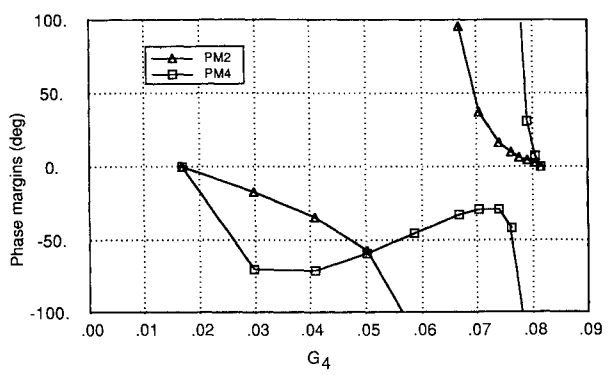

Fig. 7 Phase margins along the design path.

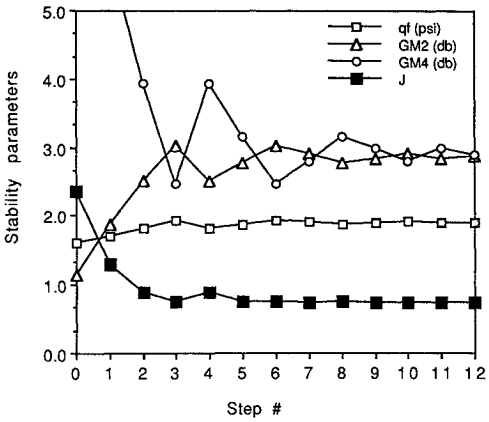

Fig. 8 Variations of flutter dynamic pressure, critical gain margins, and the objective function along the design path.

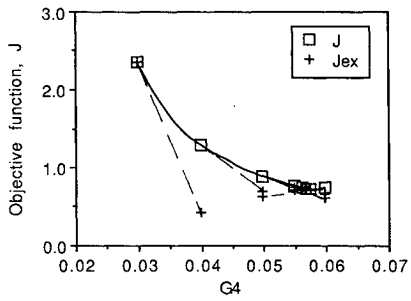

Fig. 9 Variation of the objective function vs G_4.

where FM and GM_i are the flutter and gain margins defined in Eqs. (10) and (11). The derivatives of J with respect to the independent design variables are

$$\frac{\partial J}{\partial \tilde{G}_i} = -\frac{0.1}{q_d FM^2}\frac{\partial q_f}{\partial \tilde{G}_i} - \frac{1}{GM_m^2}\frac{\partial GM_m}{\partial \tilde{G}_i}, \qquad i = 1,3,4 \quad (43)$$

where the derivatives on the right side are found by employing Eqs. (18), (31), (35), and (41). Since Eq. (42) requires the start point to be stable at q_d, the initial set of margins is chosen to be that of the end of the second step in the previous design case, namely $\{G\} = \{0, -0.135, 0, 0.03\}$. The design process is programmed to minimize J by performing steepest-descent steps. The initial step size is 0.01. This value is divided by 2 every time $J_n > J_{n-1}$.

The design process is first performed with $G_1 = G_3 = 0$ (as in the preceding case). The variations of q_f, GM_2, GM_4, and J with the design steps are shown in Fig. 8. The end-point control gains and the associated flutter dynamic pressure, critical stability margins, and objective function are compared in Table 3 to those of the preceding design case and the case discussed below. It can be observed that the process converges to the gain set just predicted. The variation of J with G_4 in the range of the design process is shown in Fig. 9. The dashed lines, which connect J_n values with those expected for J_{n+1} based on the derivatives of J, demonstrate the accuracy of the flutter and gain margin derivatives.

The last design case is now repeated with the same objective function, initial gains, and step size but with all the independent variables, G_1, G_3, and G_4, allowed to change simultaneously. The end-point results given in the last column of Table 3 show that the activation of the leading-edge control surfaces slightly alleviate the trailing-edge ones and increases the flutter and the critical gain margins by 8 to 13%. It is up to the vehicle designer in this case to decide whether these changes are worth complicating the control system by activating all four control surfaces for roll maneuvering. Another approach would be to use the end-point gains of the second case in Table 3 as a baseline for designing a higher order control system and/or performing structural modifications to increase the flutter and stability margins. This approach could be performed with the derivatives and design methodology of this paper but is beyond the scope of this application.

Table 2 Design start-point control gains and associated flutter derivatives

Control surface no.	G_i, rad-s/rad	$\partial q_f/\partial G_i$	$\partial q_f/\partial \tilde{G}_i$
1	0	−0.31	−1.27
2	−0.124	4.14	—
3	0	1.23	0.22
4	0	7.60	6.08

Table 3 End-point results of the three design cases

	Strategy		
	Maximize q_f	Minimize J with $G_1 = G_3 = 0$	Minimize J
G_1 [rad/(rad/s)]	0	0	−0.049
G_2 [rad/(rad/s)]	−0.150	−0.145	−0.143
G_3 [rad/(rad/s)]	0	0	0.045
G_4 [rad/(rad/s)]	0.070	0.057	0.054
q_f (psi)	2.005	1.896	1.930
FM	0.336	0.264	0.286
GM_2 (dB)	3.54	2.89	3.26
GM_4 (dB)	1.27	2.90	3.26
PM_2 (deg)	34.5	−97.5	−105.1
PM_4 (deg)	−29.2	−49.3	−52.4
J	1.090	0.727	0.656

Conclusions

The analytical sensitivity derivatives developed in this paper advance the automated aeroservoelastic design technology by facilitating efficient inclusion of flutter characteristics and stability margins in the objective function. Being based on state-space form, time-domain, constant-coefficient formulation, the derivatives can be implemented in modern control design algorithms. The derivative expressions can be directly applied to any design variable with respect to which the real-valued system matrix derivative is available. The developed derivatives with respect to structural and control variables facilitate application to simultaneous structural and control system design. The numerical application demonstrates the accuracy of the derivatives and their efficient usage in a case where the flutter mechanism changes during the design process. The example also demonstrates the application of design constraints and the importance of simultaneous consideration of flutter margins and gain margins.

References

[1]Bisplinghoff, R. L., and Ashley, H., *Principles of Aeroelasticity*, Wiley, New York, 1962, Chap. 9.

[2]Rudisill, C. R., and Bhatia, K. G., "Optimization of Complex Structures to Satisfy Flutter Requirements," *AIAA Journal*, Vol. 9, No. 8, 1971, pp. 1487-1491.

[3]Wilkinson, K., Lerner, E., and Taylor, R. F., "Practical Design of Minimum-Weight Aircraft Structures for Strength and Flutter Requirements," *Journal of Aircraft*, Vol. 13, No. 8, 1976, pp. 614-624.

[4]Wilkinson, K., Markowitz, J., Lerner, E., George, D., and Batill, S. M., "FASTOP: A Flutter and Strength Optimization Program for Lifting-Surface Structures," *Journal of Aircraft*, Vol. 14, No. 6, 1977, pp. 581-587.

[5]Adams, W. M., Jr., Tiffany, S. H., Newsom, J. R., and Peele, E. L., "STABCAR—A Program for Finding Characteristic Roots of Systems Having Transcendental Stabilility Matrices," NASA T.P. 2165, June 1984.

[6]Tiffany, S. H., and Adams, W. M., Jr., "Nonlinear Programming

Extension to Rational Approximation Methods of Unsteady Aerodynamic Forces," NASA TP-2776, July 1988.

[7]Karpel, M., "Design for Active and Passive Flutter Suppression and Gust Alleviation," NASA CR-3482, Nov. 1981.

[8]Karpel, M., "Time-Domain Aeroservoelastic Modeling Using Weighted Unsteady Aerodynamic Forces," *Journal of Guidance, Control, and Dynamics,* Vol. 13, No. 1, 1990, pp. 30-37.

[9]Abel, I., Newsom, J. R., and Dunn, H. J., "Application of Two Synthesis Methods for Active Flutter Suppression on an Aeroelastic Wing-Tunnel Model," *A Collection of Technical Papers—AIAA Atmospheric Flight Mechanics Conference for Future Space Systems,* AIAA, Aug. 1979, pp. 93-103.

[10]Mukhopadhyay, V., Newsom, J. R., and Abel, I., "A Method for Obtaining Reduced-Order Control Laws for High-Order Systems Using Optimization Techniques," NASA TP 1876, Aug. 1981.

[11]Zeiler, T. A., and Weisshaar, T. A., "Integrated Aeroservoelastic Tailoring of Lifting Surfaces," *Journal of Aircraft,* Vol. 25, No. 1, 1988, pp. 76-83.

[12]Sobiesczanski-Sobieski, J., James, B., and Dovi, A., "Structural Optimization by Multilevel Decomposition," *AIAA Journal,* Vol. 23, No. 11, 1985, pp. 1775-1782.

[13]Sheena, Z., and Karpel. M., "Static Aeroelastic Analysis Using Aircraft Vibration Modes," *Collected Papers of the Second International Symposium on Aeroelasticity and Structural Dynamics,* April 1985, pp. 229-232.

[14]Karpel. M., and Sheena, Z., "Structural Optimization for Aeroelastic Control Effectiveness," *Journal of Aircraft,* Vol. 25, No. 11, 1988, pp. 493-495.

[15]Kailath, T., *Linear Systems,* Prentice-Hall, Englewood Cliffs, NJ, 1980.

Candidates Solicited for *JA* Editor-in-Chief Post

On January 1, 1991, AIAA will appoint an Editor-in-Chief of its *Journal of Aircraft (JA)* for a three-year term and solicits candidates for this prestigious editorial post.

Several goals have been established for *JA* beginning in FY'91:

- To serve the largest primary interest group of AIAA members—the field of aeronautics. Many of the technical areas listed in the scope (printed below) are not currently represented in the contents of the journal.
- To increase by 50% the number of papers published in *JA* by the end of FY'91 (with no reduction in quality).
- To make *JA* the first choice of submitting authors.
- To increase significantly the number of foreign papers published, particularly from Western Europe and Japan. The USSR is moving up quickly in many areas. Emphasis should be given to research that is more advanced than that in the United States.

We are soliciting applications for the Editor-in-Chief position because of these major changes in the goals for *JA*. The term of the current Editor-in-Chief, Thomas M. Weeks, expires on December 31, 1990. Dr. Weeks has been invited to apply.

The person recommended by the selection committee must convince them of his/her desire and ability to meet the goals outlined above.

The selection committee will be chaired by Allen E. Fuhs, former Vice President—Publications and *JA* Editor-in-Chief. Other members of the committee include Roy Lange, Daniel Raymer, and Charles Sprinkle.

To apply for the editorship, submit four copies of an application citing qualifications, your objectives for the journal, and how you will meet the above goals. Send them to

Dr. Allen E. Fuhs
c/o Norma J. Brennan
AIAA Headquarters
370 L'Enfant Promenade, S.W.
Washington, DC 20024-2518

*The deadline for applications is **June 1, 1990.*** The selection committee will recommend a candidate by August 1 for approval by the AIAA Board of Directors later in August.

JA now has the following scope:

"This Journal is devoted to the advancement of the science and technology of airborne flight through the dissemination of original archival papers describing significant advances in aircraft, the operation of aircraft, and applications of aircraft technology to other fields. The Journal publishes qualified papers on aircraft systems and advanced concepts in aircraft design, flight mechanics, flight testing; flight safety, weather hazards, human factors, airport design, airline operation; air traffic control; application of computers to aircraft; aircraft-oriented information systems; production methods; engineering economic analyses; reliability, maintainability, and logistics support; the integration of propulsion and control systems into aircraft design and operations; aircraft aerodynamics, structural design, and testing. It covers papers on general aviation; military as well as civilian aircraft; ground-effect machines; STOL and V/STOL airplanes; and supersonic, transonic, and hypersonic airplanes. Papers also are sought which definitively review the results of recent technical work from the standpoint of practical engineering."

Duties of the Editor-in-Chief encompass the following: Foreseeing and stimulating major contributions to the journal, with assistance from Associate Editors and an Editorial Advisory Board; logging in, acknowledging, and appraising submitted manuscripts; checking their general quality, importance to the technical community, and compliance with editorial specifications; assigning them to Associate Editors for processing; arbitrating editorial disputes; tracking manuscripts and Associate Editor actions via computer.

The post carries an honorarium of $275 per month and reimbursement for certain allowable expenses.

Address questions about editing procedures or other factors connected with duties to Norma Brennan, AIAA Director, Editorial and Production Departments (202-646-7482).

Questions concerning policy may be directed to me in writing at the following address: Dr. Billy M. McCormac, AIAA Vice President—Publications, 91-01/B282, Lockheed R&DD, 3251 Hanover Street, Palo Alto, CA 94304.

B.M.M.